Iranian Journal of Physics Research, Vol. 25, No. 3, 2026
DOI: 10.47176/ijpr.25.3.21854

Investigation of the structural and electrical properties of Lanthanum and Samarium co-doped Ceria for low temperature solid oxide fuel cell electrolytes application

Lemessa Asefa Eressa
Department of Physics, College of Natural & Computational Sciences, Ambo University, Ambo, Ethiopia.

Email: lemessaphys@gmail.com, lemessa.asefa@ambou.edu.et

(Received 28 February 2024 ; in final form 16 March 2025)

Abstract
The aim of this study is to investigate the structural, morphological, and electrical properties of ceria co-doped with samarium and lanthanum (LSDC) for application as an electrolyte in solid oxide fuel cells operating at lower temperatures. To assess the crystal structure, microstructure, and electrical characteristics, techniques including X-ray diffraction (XRD), scanning electron microscopy (SEM), and impedance spectroscopy were employed. The findings from XRD indicated that all samples crystallized into a single-phase, cubic fluorite structure, with crystallite sizes ranging from 20 to 29 nm. Confirmation of grain formation, along with average grain sizes between 380 and 966 nm, as well as the presence of pores, is determined by the SEM micrograph. The conductivity values determined through impedance spectroscopy for the compositions $Ce_{0.9}Sm_{0.05}La_{0.05}O_{1.95}$, $Ce_{0.85}Sm_{0.05}La_{0.1}O_{1.925}$, $Ce_{0.85}Sm_{0.1}La_{0.05}O_{1.925}$, and $Ce_{0.8}Sm_{0.1}La_{0.1}O_{1.9}$ were $4.28x10^{-3}$ S/cm, $6.5x10^{-3}$ S/cm, $1.63x10^{-2}$ S/cm, and $1.13x10^{-2}$ S/cm, respectively, at a temperature of 500 ^{0}C in an air atmosphere. The activation energies calculated for the samples $Ce_{0.9}Sm_{0.05}La_{0.05}O_{1.95}$, $Ce_{0.85}Sm_{0.05}La_{0.1}O_{1.925}$, $Ce_{0.85}Sm_{0.1}La_{0.05}O_{1.925}$, and $Ce_{0.8}Sm_{0.1}La_{0.1}O_{1.9}$ are 0.83 eV, 0.76 eV, 0.64 eV, and 0.67 eV, respectively. Among the LSDC-series samples, the composition $Ce_{0.85}Sm_{0.1}La_{0.05}O_{1.925}$ exhibits the highest ionic conductivities and the lowest activation energies across all measured temperatures. Additionally, every LSDC sample demonstrated ionic conductivities greater than 10^{-3} S/cm, even at the reduce temperature of 400 °C. These results collectively validate that the co-doping of samarium and lanthanum in ceria enhances its structure, morphology, and ionic conductivity, making it a viable strong electrolyte for applications in low-temperature solid oxide fuel cells.

Keywords: LT-SOFC; electrolyte; ceria; co-doping; electrical properties.

1. Introduction

Solid oxide fuel cells (SOFCs) represent a promising electrochemical technology that converts chemical energy into electrical energy through simple redox reactions with minimum carbon emissions [1-9]. However, most SOFCs have been operated at very high temperatures (800-1000 °C), which in turn limits their applications [10]. Currently, the development of SOFCs focuses on reducing the operating temperature to medium temperatures (500-800 °C) and low temperatures (300-500 °C) [11]. As a result, the operating temperature was reduced to low temperatures (300–500 °C) and medium temperatures around 500–800 °C, leading to improved performance and subsequent commercialization of SOFCs as portable power sources [12]. However, lowering the operating temperature will result in a drop in the rate of electrocatalytic processes and an increase in electrolyte resistance [13]. Finding a different electrolyte with quick ion transport in the material is one way to overcome these difficulties [14]. Additionally, lowering the fuel cell's operating temperature is becoming more and more crucial to extending the stability and lifespan of a SOFC. Additionally, expanding the range of electrolyte materials can lower the cost of cell production and material processing. Rare earth doped ceria-based materials have a better ionic conductivity at relatively lower temperatures and a lower activation energy than YSZ electrolyte [15]. Previously, the performance of single lanthanum doped ceria electrolyte was investigated for solid oxide fuel cell application in the intermediate temperature range (550-700 ^{0}C) [16, 17]. However, literature results show that single-doped ceria-based oxides have limitations on their application as solid electrolytes due to their tendency to reduce. Ce^{4+}(ionic conduction) to Ce^{3+}(electronic conduction).

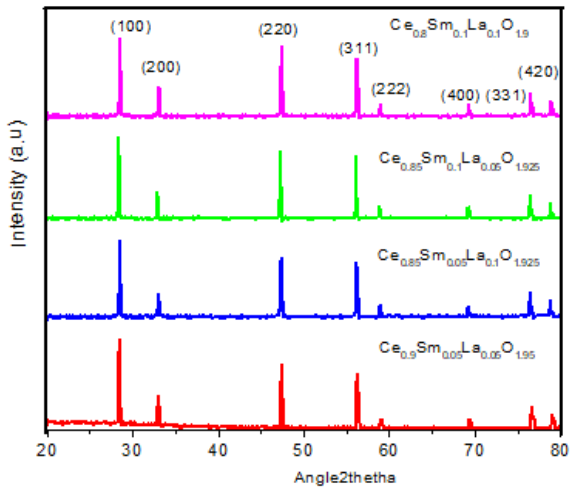

Figure 1. XRD patterns of LSDC- samples

Moreover, at low operating temperatures, grain boundary resistance is a significant inhibition to ionic conductivity [18]. Thus, research results showed that co-doping strategy is another option to improve the electrical properties of ceria based electrolytes at low temperature range by decreasing grain resistance and minimizing reduction of ceria [19, 20]. Therefore, the author aimed to have comprehensive investigation of structural, morphology and electrical properties of lanthanum and samarium co-doped ceria($Ce_{1-x-y}Sm_xLa_yO_{2-\delta}$ ($0.0 \leq x = y \leq 0.05,0.1$) for use as an electrolyte for low temperature solid oxide fuel cell (LT-SOFC) applications.

2. Experimental Methods

In this study, cerium nitrate hexahydrate ($Ce(NO_3)_3.6H_2O$)) 99.99% purity, Samarium nitrate hexahydrate (($Sm(NO_3)_3.6H_2O$)) 99.99% purity, Lanthanum (III) nitrate hexahydrate (($La(NO_3)_3.6H_2O$)) 99.99% purity, Ammonium hydroxide (NH_4OH), Citric acid ($C_6H_8O_7$), Ethylene glycol (($CH_3COOC_2H_5$) were used as starting chemicals for the preparation of LSDC samples using sol-gel method. Initially, stoichiometric amounts of all nitrates were dissolved in distilled water under continuous stirring. Next, citric acid was added to the entire mixture of precursors in 1:1 molar ratio to take care of the entire molar ratio of metal to acid. So as to regulate the pH value to (*p*H to ≈7), ammonium hydroxide was added drop by drop to the solution. Further, the entire mixture was stirred at 80 ^{0}C for 3hours to make a homogenous solution. After 3hours, a viscous gel was formed which in turn placed in an oven to make an ash. Ash was calcined at 600 ^{o}C for 2 hours to get rid of the carbonaceous materials. The resultant ash was ground continuously for 1hour in agate mortar to get a fine homogeneous powder. The powders were pressed with the help of a hydraulic press under a pressure of 200 MPa into a circular pellet (8mm in diameter and 2 mm in thickness). Finally, the pellets were sintered in furnace at 1400 ^{o}C for 2hours and prepared for impedance measurement.

3. RESULT AND DISCUSSION

3.1 Structural Characterization by X-ray Difrractometer

The structural characterization of all the sintered LSDC samples were done at room temperature using Philips X-ray Diffractometer with Cuk_α radiation (λ=1.54 A^0) operated at 40 kV and 30 mA in the 2θ range of 20–80° with a step size of 0.02 and a time for step is 2s. Figure 1 illustrates the X-ray diffraction data of prepared samarium and lanthanum co-doped ceria samples. X-ray diffraction patterns of all the samples indexed to (hkl) parameters i.e. (111), (200), (220), (311), (222), (400), (331) and (420) indicating the formation of each composition with single phase cubic structure with JCPDS PDF: 34–0394 and space group Fm3m [21-23]. This confirms that no diffraction peaks resulting from impurity phases were observed in all LSDC samples, suggesting the formation of a homogeneous single polycrystalline phase.

The differences in ionic radius i.e. higher ionic radius of dopants compared to cerium lead to an increase in the lattice parameter values with increase in the dopant concentration, which is validated by the shift in powder X-ray diffraction (PXRD) patterns [24, 25]. The variation in the lattice parameter values with the composition were determined from the rietveld refinements of PXRD patterns. The crystallographic information i.e., crystal structure, lattice parameter and crystallite sizes of all the co-doped ceria samples were listed in Table 1.

Scherer equation is used to determine the crystallite size (D) from the PXRD data (i.e. (111) plane of reflection) of all the samples

$$D = \frac{0.9\lambda}{\beta cos\theta} \quad (1)$$

Where K is the shape factor, λ is the wavelength, θ is the diffraction angle and β is the full
width half maxima. Table 1 describes the calculated crystallite sizes for each sample, which were all found to fall between 20 and 29 nm. This phenomenon suggests improvements in the crystallite size as a result of co-doping strategy.

3.2. Morphology Characterization by Scanning Electron Microscope

The morphology of sintered $Ce_{1-x-y}Sm_xLa_yO_{2-\delta}$ pellets was taken by field-emission scanning electron microscope (FE-SEM, Carl Zeiss, EVO18). Figure 2 presents the SEM images of all the samples sintered at 1400 °C for 2 hours with grains showing some pores. Calculations revealed that the average grain sizes of all the LSDC samples were in the range of 380 and 966 nm and indicated in Table 1. The ionic radius variation between the co-dopants samarium and lanthanum, as well as their concentrations, is what causes the diversity in grain size seen among samples. Additionally, it was produced as a result of their dissimilar morphologies, which led to uneven temperature treatments during sample synthesis.

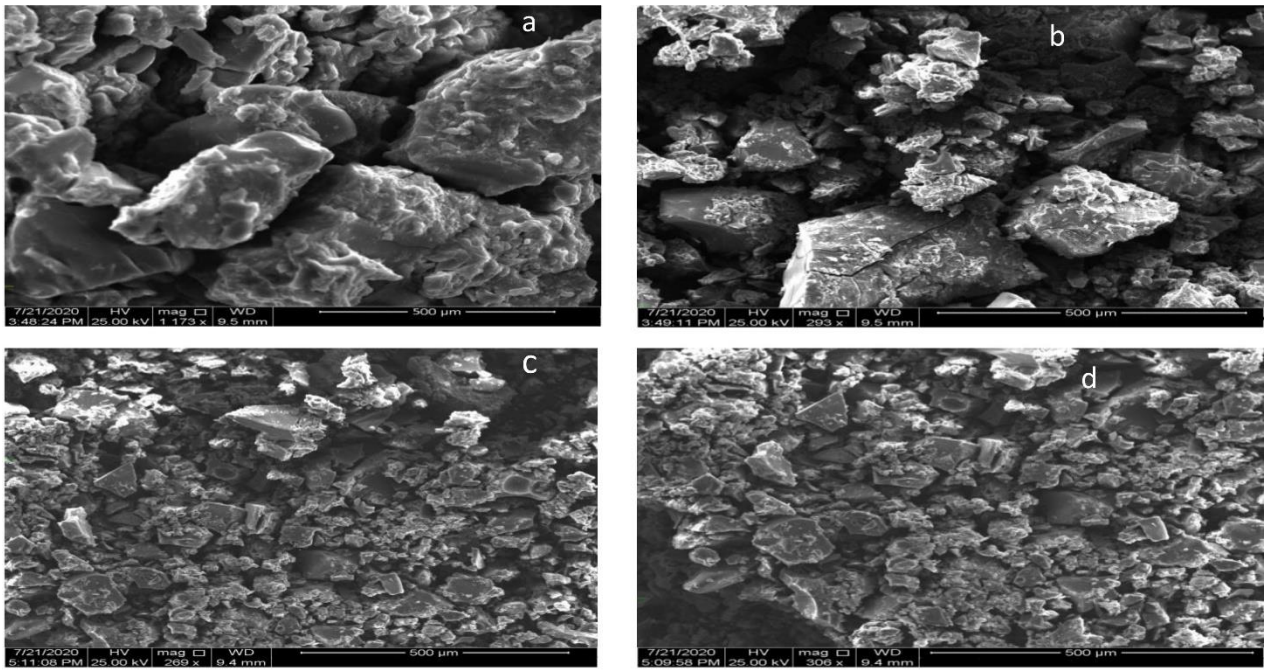

Figure 2. SEM graphs of (a) $Ce_{0.9}Sm_{0.05}La_{0.05}O_{1.95}$ (b) $Ce_{0.85}Sm_{0.05}La_{0.1}O_{1.92\,5}$ (c) $Ce_{0.85}Sm_{0.1}La_{0.05}O_{1.925}$ (d) $Ce_{0.8}Sm_{0.1}La_{0.1}O_{1.9}$

Table 1 Crystallite size, grain size and lattice parameter of LSDC-samples

No.	Compositions	Crystallite Size (nm)	Grain Size (nm)	Lattice Parameter (Å)
1	$Ce_{0.9}Sm_{0.05}La_{0.05}O_{1.95}$	29	966	5.414
2	$Ce_{0.85}Sm_{0.05}La_{0.1}O_{1.925}$	26	840	5.416
3	$Ce_{0.85}Sm_{0.1}La_{0.05}O_{1.925}$	21	620	5.418
4	$Ce_{0.8}Sm_{0.1}La_{0.1}O_{1.9}$	20	380	5.417

Table 2. Resistances and conductivities of $Ce_{0.9}Sm_{0.05}\ La_{0.05}O_{1.95}$ sample

Temperature(^{0}C)	$\boldsymbol{Rg(\Omega}$	$\boldsymbol{Rgb(\Omega}$	$\boldsymbol{R(\Omega}$	$\boldsymbol{\sigma(S/cm)}$
400	145.7	581.3	727	$1.1x10^{-3}$
450	117.38	227.81	345.19	$2.32x10^{-3}$
500	55.06	131.99	187.05	$4.28x10^{-3}$

Table 3.Resistances and conductivities of $e_{0.85}Sm_{0.05}La_{0.1}O_{1.925}$ sample

Temperature(^{0}C)	$\boldsymbol{Rg(\Omega}$	$\boldsymbol{Rgb(\Omega}$	$\boldsymbol{R(\Omega}$	$\boldsymbol{\sigma(S/cm)}$
400	131.2	215.9	347.1	$2.3x10^{-3}$
450	90.38	99.39	189.77	$4.2x10^{-3}$
500	42.27	81.6	123.87	$6.5x10^{-3}$

Table 4. Resistances and conductivities of $Ce_{0.85}Sm_{0.1}La_{0.05}O_{1.925}$ sample

Temperature(^{0}C)	$\boldsymbol{Rg(\Omega}$	$\boldsymbol{Rgb(\Omega}$	$\boldsymbol{R(\Omega}$	$\boldsymbol{\sigma(S/cm)}$
400	28.5	52.3	80.8	$9.9x10^{-3}$
450	25.01	27.32	52.33	$1.52x10^{-2}$
500	22.54	26.56	49.1	$1.63x10^{-2}$

Table 5. Resistances and conductivities of $Ce_{0.8}Sm_{0.1}\ La_{0.1}O_{1.9}$ sample

Temperature(^{0}C)	$\boldsymbol{Rg(\Omega}$	$\boldsymbol{Rgb(\Omega}$	$\boldsymbol{R(\Omega}$	$\boldsymbol{\sigma(S/cm)}$
400	36.9	65.4	102.3	$7.82x10^{-3}$
450	34.00	45.12	79.12	$1.01x10^{-2}$
500	30.02	40.39	70.39	$1.13x10^{-2}$

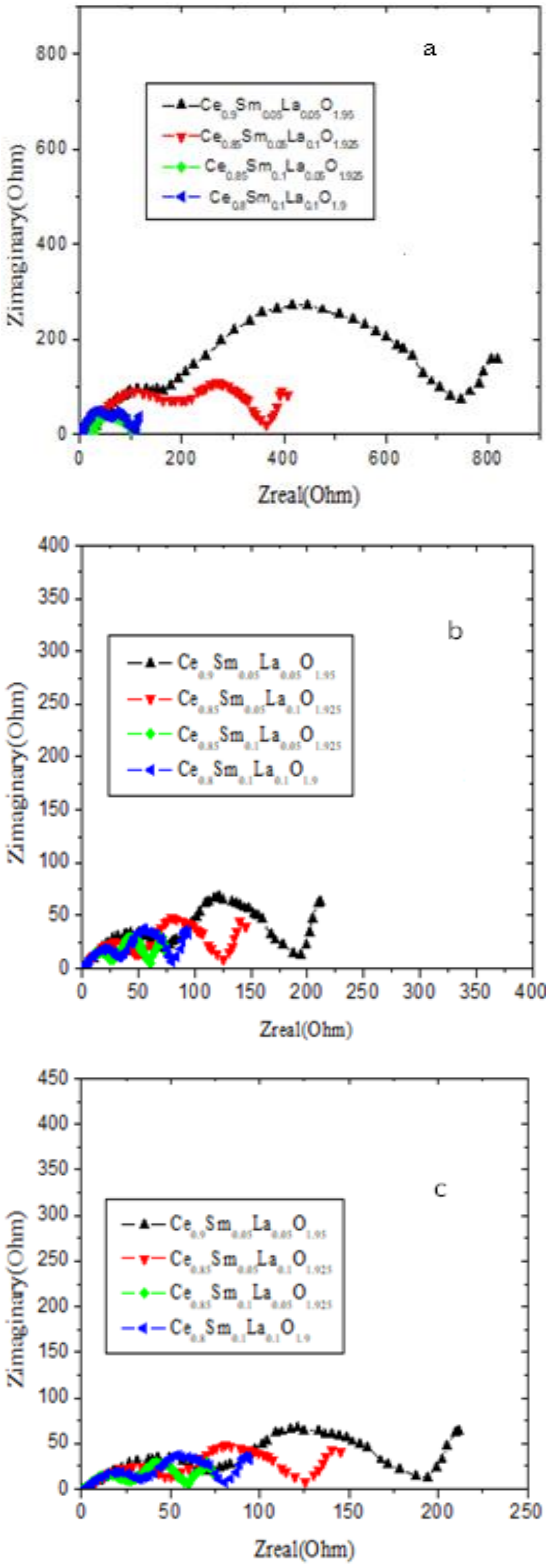

Figure 3. Nyquist Plots of LSDC-Samples at Temperatures of a) 400 ^{0}C b) 450 ^{0}C and c)500 ^{0}C.

3.3. Electrical analysis

AC impedance measurements were carried out on pellets coated with silver paint on both surfaces employing Auto lab impedance Analyser in the frequency range 1Hz-1MHz and from room temperature to 500°C. The impedance spectra consist of graphs with real part Z' on X-axis and negative imaginary part Z'' on Y-axis known as complex impedance spectra and is a materials characteristic conducting nature [26-28]. In many cases, complex impedance spectra characterized by three successive semi-circle contributions; lower frequency semi-circle is corresponds to electrode contribution, medium frequency semi-circle corresponds to grain boundary contribution and the higher frequency semi-circle corresponds to grain contribution [29, 30] The complex impedance analysis of lanthanum and samarium co-doped ceria samples was carried out in the temperature range from 400 to 500 °C.

Figure 3 (a), (b) and (c) represents the complex impedance plots at 400 °C, 450 °C and 500 °C respectively for co-doped ceria samples with a combination of three semi-circles correspond to grain, grain-boundary and electrode contributions. As it can be observed form figure 3 (a), (b) and (c), the curves seem to be clear semicircles. With the increase in the concentration and temperature, the semi-circles were decreased gradually in size. The clear semi-circles were observed only when homogeneous grain size distribution and grain shapes present in the co-doped ceria ceramics. As the temperature increases, the area under the semi-circle decreases. This resulted in the decrease of the impedance which in turn leads to an increase in the conductivity. The area under the semicircles also decreased with increase in the temperature and the area under the semi-circle found to be the least for the composition $Ce_{0.85}Sm_{0.1}La_{0.05}O_{1.925}$ at all temperatures among LSDC samples. This indicates, the decrease in the impedance of the samples leads to an increase in the conductivity. At higher temperature, the complex impedance plots not show any arc at the lower frequency region and this observation recommends virtually that there is no contribution of electrode process to the electrical conductivity [26, 31, 32].

The total resistance (sum of grain and grain-boundary resistance i.e. R_T = Rg+Rgb) of all the samples, at all temperatures were calculated from the intercepts of semi-circle on the real impedance axis [32-34]. The total resistance is given by

$$R_T = R_g + R_{gb} \quad (2)$$

where *R*g and *R*gb stand for the resistance of grain interior and grain boundary respectively.

Then, the ionic conductivity (σ) of each sample was calculated using the equation

$$\sigma = \frac{l}{RA} \quad (3)$$

where l is the thickness of sample and A is the cross-sectional area. Through curve fitting a circle to the semi circles on the impedance spectra, the sample total resistance (R) was obtained using equation (2). Then, the conductivity values of samples were calculated from the resistance values using equation (3). This result presented in Tables 2, 3, 4 and 5 below.

As indicated in Tables 2, 3, 4 & 5, the conductivity of compositions $Ce_{0.9}Sm_{0.05}La_{0.05}O_{1.95}$, $Ce_{0.85}Sm_{0.05}La_{0.1}O_{1.925}$, $Ce_{0.85}Sm_{0.1}La_{0.05}O_{1.925}$ and $Ce_{0.8}Sm_{0.1}La_{0.1}O_{1.9}$ obtained were $4.28x10^{-3}$S/cm, $6.5x10^{-3}$S/cm, $1.63x10^{-2}$S/cm and $1.13x10^{-2}$S/cm respectively at 500 ^{0}C in air atmosphere.

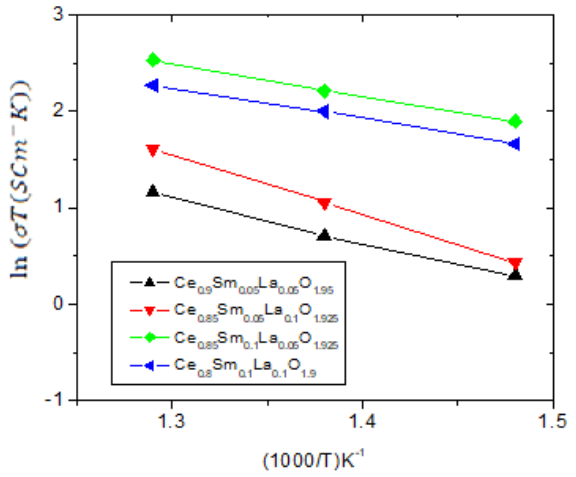

Figure 4. Arrhenius plots for total conductivity of LSDC-samples

Table 6. Activation energy of LSDC- samples

No	Sample	Ea(*eV*)
1	$Ce_{0.9}Sm_{0.05}La_{0.05}O_{1.95}$	0.83
2	$Ce_{0.85}Sm_{0.05}La_{0.1}O_{1.925}$	0.76
3	$Ce_{0.85}Sm_{0.1}La_{0.05}O_{1.925}$	0.64
3	$Ce_{0.8}Sm_{0.1}La_{0.1}O_{1.9}$	0.67

Generally, the higher dopant concentration, the higher concentration of mobile ion (ion oxide vacancy) that leads to the higher ionic conductivity. For co-doped ceria with the ratio of Sm^{3+} (r= 1.08A^0) dopant and La^{3+} (r= 1.16A^0) dopant was 1:1. The conductivity of $Ce_{0.8}Sm_{0.1}La_{0.1}\ O_{1.9}$ was higher than $Ce_{0.9}Sm_{0.05}La_{\ 0.05}\ O_{1.95}$ .This happens due to the greater lattice parameter of $Ce_{0.8}Sm_{0.1}La_{0.1}\ O_{1.9}$ (5.417 **Å**) which in turn facilitates fast diffusion of oxygen ions contributing greater ionic conductivity than in $Ce_{0.8}Sm_{0.1}La_{0.1}\ O_{1.9}$ which has smaller lattice parameter of 5.414 **Å.** On the other hand, for co-doped ceria with total dopants concentration of 15% or the ratio between Sm^{3+} dopant and La^{3+} was 1:2 or 2:1, the conductivity of $Ce_{0.85}Sm_{0.1}La_{0.05}O_{1.925}$ is greater than conductivity of $Ce_{0.85}Sm_{0.05}La_{0.1}O_{1.925}$. That means, further increasing of the lanthanum concentration leads to the formation of ion clusters which results in the deep traps to oxygen vacancies results in lowering the concentration of oxygen vacancies ultimately decrease the ionic conductivity of the sample. This is created as a result of big difference between the ionic radii of La^{3+} (1.16 Å) than Ce^{4+}(0.970Å) which is consistent with literature reports [23]. But, increasing concentration of Sm^{3+} into ceria increases the total conductivity. That means, the ionic conductivity of $Ce_{0.85}Sm_{0.1}La_{0.05}\ O_{1.925}$ was higher than $Ce_{0.85}Sm_{0.05}La_{\ 0.1}O_{1.925}$. This due to the ionic radii of Sm^{3+} which is more close to the critical ionic radii (1.038A^0) than ionic radii of lanthanum [35]. This property enhances the mobility of oxygen vacancies contributing highest ionic conductivity in $Ce_{0.85}Sm_{0.1}La_{0.05}\ O_{1.925}$ than in $Ce_{0.85}Sm_{0.05}La_{\ 0.1}O_{1.925}$ sample.

The temperature dependence of ionic conductivity often follows an Arrhenius relation

$$\sigma T = \sigma_o e^{-Ea/KT} \qquad (4)$$

where Ea is the activation energy for conduction, T is the temperature, k is the Boltzmann's constant and σ_o is a pre-exponential factor. The total ionic conductivities of LSDC- samples sintered at 1400^{0}C for 2hours was presented in figure 4 in the form of $\ln(\sigma T)$ versus (10^3/T). The value of Ea and σ_o were found from the slope and intercept of the graph respectively.

The Arrhenius plot described in figure 4 reveals that the conductivity of all the LSDC-samples increased exponentially with temperature. This was possibly because of thermal excitation which enhances the kinetic energy of carriers and force oxygen ions to pass through oxygen vacancies in a higher speed. As the temperature rises, there exists stronger diffusion ability of oxygen ions, which ultimately lead to the enhancement of conductivity.

As it can be observed from figure 4, the graph of $Ce_{0.85}Sm_{0.1}La_{0.05}O_{1.925}$ lies above the graphs of other LSDC-samples. This shows that the conductivity of $Ce_{0.85}Sm_{0.1}La_{0.05}O_{1.925}$ sample is the highest of all the other LSDC-samples. This could be due to formation of more number of oxygen vacancies and suppression of ordering of oxygen vacancies in $Ce_{0.85}Sm_{0.1}La_{0.05}O_{1.925}$ than in other LSDC-samples. This phenomena leads to a decrease in the activation energy for diffusion of O^{2-} ions in $Ce_{0.85}Sm_{0.1}L_{0.05}O_{1.925}$ sample.

Double doping lanthanum and samarium in ceria increases the oxygen vacancy disorder which helps to improve the grain conductivity. The increase of lattice constant caused by optimum lanthanum doping enlarges the channel of oxygen ion transport which also improves the grain conductivity. However, lattice distortion may occur with further increase in lanthanum content due to the big difference between the ionic radii of La^{3+} (1.16 Å) than Ce^{4+}(0.970Å) as reported in previous literature [36].

Table 6 shows that the activation energy of LSDC-samples obtained by fitting of the data in Figure 3 to Arrhenius relations equation (4). In this study, the calculated activation energies of samples $Ce_{0.9}Sm_{0.05}La_{0.05}O_{1.95}$, $Ce_{0.85}Sm_{0.05}La_{0.1}O_{1.925}$, $Ce_{0.85}Sm_{0.1}La_{0.05}O_{1.925}$ and $Ce_{0.8}Sm_{0.1}La_{0.1}O_{1.9}$ were 0.83eV, 0.76eV, 0.64eV and 0.67eV respectively. The activation energy of $Ce_{0.85}Sm_{0.1}La_{0.05}O_{1.925}$ has the least activation energy which results with the greatest diffusion of oxygen ions (greatest ionic conductivity) in the sample than other LSDC sample series at all measurements.

In general, the addition of trivalent elements (La^{3+} and Sm^{3+}) to the structure of pure ceria often resulted in an increase in the value of the crystal lattice parameter of LSDC- samples. As a result, the unit cell expands and oxygen vacancies are created, which are necessary for the conduction process. This facilitates the movement of oxygen ions and reduces the resistances of the grains and grain boundaries. All these factors ultimately resulted in an increase in the ionic conductivity and lowering of activation energy of the LSDC-samples. Hence, co-doping strategy is a good method in improving the structural and electrical properties of LSDC- samples at low temperature. This may be due to increase in the effective ionic radii of co-dopants which is close to the critical ionic radii (1.038 Å) for doped ceria [28]. As the ionic radii of these dopant cations are closer to the critical

ionic radii of host, the lower activation energy effect to the diffusion of oxygen vacancies resulted in to the greater the conductivity of the electrolyte.

Based on electrical analysis described on Tables 4 & 6, the formation of high concentrated oxygen vacancies of $Ce_{0.85}Sm_{0.1}La_{0.05}O_{1.925}$ resulted in the highest total ionic conductivity of $1.63x10^{-2}$S $cm^{-1}$with minimum activation energy of 0.64eV. In general, the conductivity of co-doped LSDC- samples obtained in the temperature range 400-500 ^{0}C in this work was higher than that of single lanthanum doped ceria previously reported [37, 38].

4. Conclusions

The advance of SOFC in lowering its operating temperature has targeted the use of electrolytes which operates at lower temperatures. In order to attain this goal, co-doping strategy was employed to samarium and lanthanum co-doped ceria electrolytes prepared through sol-gel synthesis method. The XRD result reveals that all the samples were single phase with cubic fluorite-type structure. The SEM micrograph definitely showed the presence of grains with presence of pores. The impedance spectroscopy measurements indicated that all the samples showed conductivities higher than $10^{-3}Scm^{-1}$ at low temperature range (400-500 °C). All of these results support the notion that samarium and lanthanum co-doping of ceria improved its structural and electrical properties. The findings confirmed that co-doped ceria with samarium and lanthanum is a promising electrolyte for solid oxide fuel cell at low temperature. For better work and comprehensive investigation of these material properties, performing mechanical strength tests, EDS measurements, Raman measurements, BET measurements and use of advanced impedance spectroscopy (which measures frequency up to 40MHz) were some of the recommendations made as a future work.

Data Availability Statement

The data that support the findings of the study are available within the article.

Conflicts of Interest

The author declares no conflicts of interest.

Funding

No funding was received for this research

Acknowledgments

I am gratefully acknowledged the Addis Ababa Science and Technology University (AASTU) for their support during this work.

References

1. T Changan, et al., *Journal of Rare Earths*, **32**(12) 1162-1169 (2014).
2. F -Y Wang, et al., *Catalysis Today*, **97**(2-3) 189-194 (2004).
3. N Jaiswal, et al., *Ionics*, **20** 45-54 (2014).
4. S C Singhal and K Kendall, Elsevier, 2003.
5. M D Mat, et al., *International Journal of Hydrogen Energy*, **32**(7) 796-801 (2007).
6. S Park, J M Vohs, and R J Gorte, *Nature*, **404**(6775) 265-267 (2000).
7. C Sındıraç, A Büyükaksoy, and S Akkurt, *Solid State Ionics*, **340** 115020 (2019).
8. S Costilla-Aguilar, et al., *Journal of Alloys and Compounds*, **878** 160444 (2021).
9. A Choudhury, H Chandra, and A Arora, *Renewable and Sustainable Energy Reviews*, **20** 430-442 (2013).
10. A Arabaci, *ACTA PHYSICA POLONICA A*, **137** 530-534 (2020).
11. Y Xia, et al., *International Journal of Hydrogen Energy*, **37**(16) 11934-11940 (2012).
12. S Omar, E D Wachsman, and J C Nino, *Applied Physics Letters*, **91**(14) (2007).
13. A Hardian, in 2011 2nd International Conference on Instrumentation, Communications, Information Technology, and Biomedical Engineering, IEEE, 2011.
14. L Fan, et al., *Nano Energy*, **45** 148-176 (2018).
15. I Shajahan, et al., *Materials Chemistry and Physics*, **216** 136-142 (2018).
16. K Singh, R Kumar, and A Chowdhury, *Materials Today: Proceedings*, **5**(11) 22993-22997 (2018).
17. H Sumi, et al., *Journal of Asian Ceramic Societies*, **9**(2) 609-616 (2021).
18. N K Singh, et al., *Ionics*, **18** 127-134 (2012).
19. W Zając and J Molenda, *Solid State Ionics*, **179**(1-6) 154-158 (2008).
20. B Li, et al., *Journal of Power Sources*, **195**(4) 969-976 (2010).
21. G Accardo, et al., *Ceramics International*, **44**(4) 3800-3809 (2018).
22. M Kahlaoui, et al., *Ceramics International*, **39**(4) 3873-3879 (2013).
23. K Venkataramana, et al., *Ceramics International*, **44**(6) 6300-6310 (2018).
24. K Venkataramana, et al., *Journal of Alloys and Compounds*, **719** 97-107 (2017).
25. R D Shannon, *Acta Crystallographica Section A*, **32**(5) 751-767 (1976).
26. S Ramesh and K J Raju, *International Journal of Hydrogen Energy*, **37**(13) 10311-10317 (2012).
27. K Anjaneya, et al., *Journal of Alloys and Compounds*, **578** 53-59 (2013).
28. V P Kumar, et al., *Materials Chemistry and Physics*, **112**(2) 711-718 (2008).
29. A Arabaci, *Ceramics International*, **41**(4) 5836-5842 (2015).

30. S Badwal, F Ciacchi, and D Milosevic, *Solid State Ionics*, **136** 91-99 (2000).
31. K N Kumar, et al., *Journal of Materials Science: Materials in Electronics*, **29**(2) 1153-1172 (2018).
32. Y-C Wu and C-C Lin, *International Journal of Hydrogen Energy*, **39**(15) 7988-8001 (2014).
33. A Hauch, M Mogensen, and A Hagen, *Solid State Ionics*, **192**(1) 547-551 (2011).
34. Q Hu, et al., *International Journal of Electrochemical Science*, **12**(8) 7411-7425 (2017).
35. S Omar, et al., *Journal of the American Ceramic Society*, **92**(11) 2674-2681 (2009).
36. S M. Haile, *Acta Materialia*, **51**(19) 5981-6000 (2003).
37. T Mori, et al., *Journal of the Electrochemical Society*, **150**(6) A665 (2003).
38. M Stojmenović, et al., *Journal of Materials Science*, **50** 3781-3794 (2015).